Biol Cybern (2011) 105:253–268
DOI 10.1007/s00422-011-0465-3

ORIGINAL PAPER

Biological Cybernetics

The mechanisms for compression and reflection of cortical waves

Julie Goulet · G. Bard Ermentrout

Received: 15 August 2011 / Accepted: 2 November 2011 / Published online: 22 November 2011

Abstract Waves are common in cortical networks and may be important for carrying information about a stimulus from one local circuit to another. In a recent study of visually evoked waves in rat cortex, compression and reflection of waves are observed as the activation passes from visual areas V1 to V2. The authors of this study apply bicuculline (BMI) and demonstrate that the reflection disappears. They conclude that inhibition plays a major role in compression and reflection. We present several models for propagating waves in heterogeneous media and show that the velocity and thus compression depends weakly on inhibition. We propose that the main site of action of BMI with respect to wave propagation is on the threshold for firing which we suggest is related to action on potassium channels. We combine numerical and analytic methods to explore both compression and reflection in an excitable system with synaptic coupling.

Keywords Waves · Cortex · Spiking network · Reflection

1 Introduction

There has been a great deal of recent interest in spatio-temporal activity in neural systems with particular attention to the mammalian cerebral cortex. This activity is observed using multiple electrodes, non-invasive imaging, and using direct imaging of the brain with or without voltage/calcium sensitive dyes in both intact and in brain-slice preparations. One of the most commonly observed types of activity takes the form of propagating waves (reviewed in Wu et al. 2007). In general, a wave is defined as an activity profile which is invariant under some combinations of translations or rotations in time and space. While a variety of two-dimensional waves, such as spiral and target waves have been seen (Shusterman and Troy 2008), most of the waves observed in vivo and in slices are effectively one-dimensional waves. As such, there are several classes of propagating one-dimensional waves observed in neural systems: (1) pulses; (2) fronts; and (3) wave trains. Wave trains occur rhythmically (Ermentrout and Kleinfeld 2001) and are usually a sign of underlying oscillatory activity. In contrast, pulses and fronts are "one shot" waves that travel across the tissue when evoked by some experimental stimulus. With pulse waves, the tissue returns to its original state while a front represents a change in states. True fronts are uncommon since almost all neural systems eventually return to their resting states. The classic neural example of a pulse is the propagating action potential of the Hodgkin–Huxley, Fitzhugh–Nagumo, and other reaction-diffusion models. Pulse and front waves in cortical networks are generally believed to be due to synaptic interactions since they disappear when synaptic conductances are blocked. There have been many theoretical advances in our understanding of synaptically generated waves; Coombes (2005) provides a relatively recent review of the theoretical work. Both firing rate and spiking networks (such as conductance-based models or integrate-and-fire type models) exhibit propagating waves (Bressloff 2000; Ermentrout and McLeod 1991; Golomb and Ermentrout 2001, 2002; Osan et al. 2002; Pinto and Ermentrout 2001; Prat et al. 2005). Pulse waves typically arise when the underlying medium is excitable. That is, brief perturbations decay to rest but larger perturbations result in an amplification of activity followed

J. Goulet (✉)
Physik Department T35 and Bernstein Center for Computational Neuroscience, TU München, Garching bei München, Germany
e-mail: julie@ph.tum.de

G. B. Ermentrout
Department of Mathematics, University of Pittsburgh, Pittsburgh, PA 1520, USA
e-mail: bard@pitt.edu

by a decay to rest. Front waves are usually associated with bistable media.

The cortex is not a homogeneous medium. Thus, there has been a good deal of recent interest in wave propagation in the presence of heterogeneities. Bressloff et al. (2003), Kilpatrick and Bressloff (2010), and Hutt and Atay (2006) have used a variety of methods to study propagation of neural waves in heterogeneous media. For rapidly varying media, Prat et al. (2005) have used homogenization methods to estimate mean velocity. More relevant to the present paper is that heterogeneities produces *change* in the velocity of waves and result in *propagation* failure. The issue of propagation and failure in rate models has been addressed in numerous models (Bressloff 2001; Coombes and Laing 2011; Kilpatrick et al. 2008). In a recent paper, Xu et al. (2008) studied the propagation of spontaneous and evoked activity as it travels across visual cortical areas in the rat. These experimentalists were particularly interested in mechanisms by which activity propagated from one area (V1) to another area (V2) in the cortex. They looked at waves that spontaneously occurred during the experiment as well as those evoked by a drifting grating presented to the animal. They found two phenomena as waves crossed from V1 into V2. First, when the waves were evoked by stimuli, there was compression of the wave as it entered V2 and on many occasions, secondary activity was reflected back into V1. In contrast, waves that occurred spontaneously show no compression or reflection. By compression, these authors mean that during a snapshot in time, the width of the activated area (as determined by voltage-sensitive dyes) is thinner in V2 than it is in V1. Xu et al. pharmacologically manipulate the cortical region by adding bicuculline (BMI) which (among other things) blocks GABA A (inhibitory) receptors and thus effectively reduces inhibition. Another effect of BMI is that it also blocks calcium activated potassium channels which can set the threshold for excitatory pyramidal neurons.

Reflected waves are often found in heterogenous tissue. In Ermentrout and Rinzel (1996), reflected waves were computed and analyzed geometrically in an inhomogeneous reaction-diffusion model of an excitable medium. They found that reflected waves were quite easy to obtain in certain types of excitable media but far more difficult in others. Specifically, in Rinzel and Ermentrout (1998) they suggested that there are at least two distinctive types of excitable media which are characterized by how they transition from rest to repetitive firing. In Class II excitability, the local medium has a single equilibrium point and as current (or some other parameter) is increased, the system becomes oscillatory through a Hopf bifurcation. Class I excitability is characterized by a saddle-node invariant circle bifurcation and thus has three equilibria in the excitable regime. Only the rest state is stable. A crucial aspect of class I excitability is the existence of a saddle point and its associated stable manifold (SM). Stimuli that cross this manifold result in a *spike*. An important consequence of the existence of the saddle point is that the spike can be produced with an arbitrarily long latency. The idea in Ermentrout and Rinzel (1996) is to exploit this latency as follows. Consider a wave propagating from A to B where the medium in B is less excitable than that in A. As the wave enters B, there could be a long latency to fire since it is less excitable. If the latency is long enough, then the medium in A will have recovered sufficiently to be re-excited when B fires. This results in a reflected wave.

We hypothesize that wave compression is nothing more than a slowing down of the wave and thus are interested in how the velocity of waves depends on various parameters. In Golomb and Ermentrout (2001, 2002), they explored velocity dependence in integrate-and-fire models which were restricted to spike only once. In contrast, in this paper, we consider first a *firing rate model* with excitatory and inhibitory neurons. We examine several different types of heterogeneity and whether or not these can result in reflections. We also study how velocity depends on the degree of inhibition and, in agreement with recent data, Pinto et al. (2005) show that there is only weak dependence of the velocity on the degree of inhibition. We also discuss why this should be so. Thus, we suggest that the effects seen in Xu et al. (2008) are due, not to changes in inhibition, but, rather, to modulation of the excitability of the medium through alteration of potassium channels. Next, we consider a simplified model for reflection and compression that arises as a *normal form* near a bifurcation of the population model. This allows us to better explore parameter space. We close with some simple analytic calculations that give a range of parameters for reflection to occur in a discrete chain.

2 Model

We use a firing rate model based on a combination of the Pinto–Ermentrout (disinhibited cortex) model and the Wilson–Cowan equations

$$\begin{aligned}
\frac{\partial u_{\mathrm{e}}(x,t)}{\partial t} &= -u_{\mathrm{e}}(x,t) + f\,(a_{\mathrm{ee}}(x)K_{\mathrm{e}}(x)\cdot u_{\mathrm{e}}(x,t) \\
&\quad -a_{\mathrm{ie}}(x)K_{\mathrm{i}}(x)\cdot u_{\mathrm{i}}(x,t) \\
&\quad - g_{\mathrm{a}}(x)z(x,t) - \theta_{\mathrm{e}}(x)) \\
\tau_{\mathrm{i}}\frac{\partial u_{\mathrm{i}}(x,t)}{\partial t} &= -u_{\mathrm{i}}(x,t) + f\,(a_{\mathrm{ei}}(x)K_{\mathrm{e}}(x)\cdot u_{\mathrm{e}}(x,t) \\
&\quad - a_{\mathrm{ii}}(x)K_{\mathrm{i}}(x)\cdot u_{\mathrm{i}}(x,t) - \theta_{\mathrm{i}}(x)) \\
\tau_a\frac{\partial z(x,t)}{\partial t} &= -z(x,t) + u_{\mathrm{e}}(x,t)
\end{aligned} \tag{1}$$

where

$$K_{\mathrm{e,i}}(x)\cdot u_{\mathrm{e,i}}(x,t) := \int_0^L K_{\mathrm{e,i}}(x-y)u_{\mathrm{e,i}}(y,t)\,\mathrm{d}y,$$

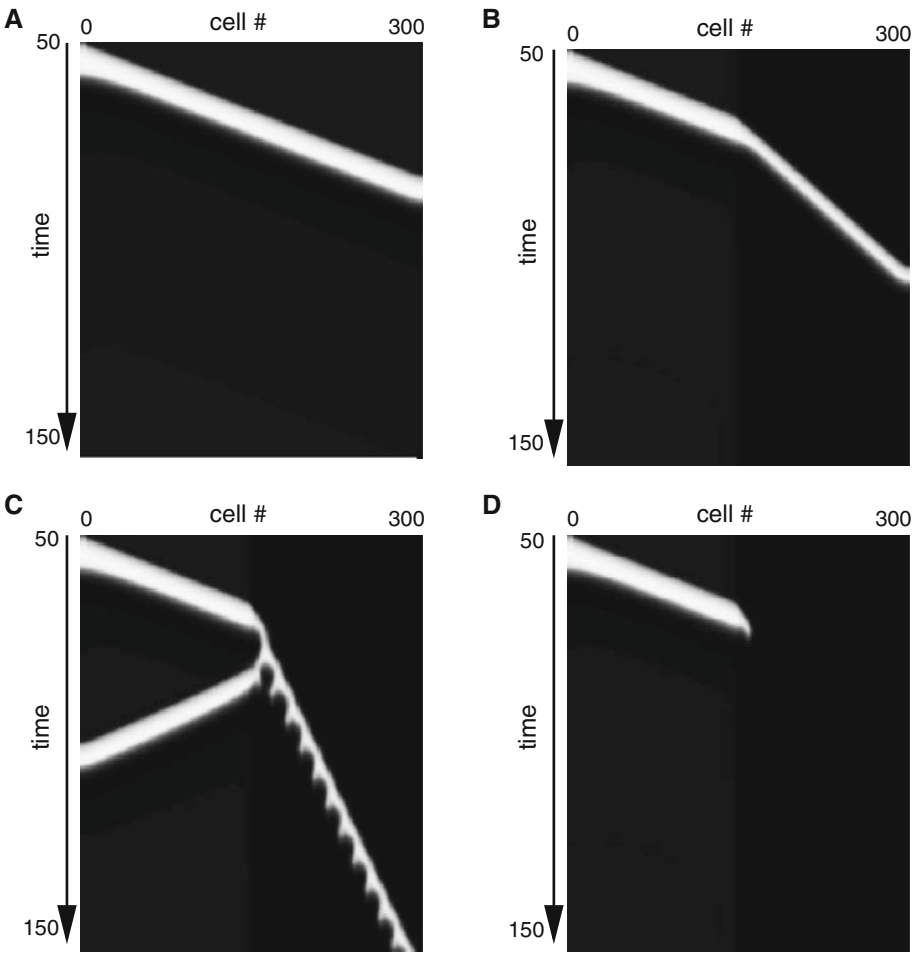

Fig. 1 Wave propagation in Eq. 1 in the homogeneous domain (**a**); and with the excitatory threshold increased in the right half of the domain by **b** 30% ; **c** 51.8%; **d** 55%. (Parameters are $\sigma_e = 4, \sigma_i = 2, a_{ee} = 20, a_{ie} = 13, g_a = 2, \theta_e = 4, a_{ei} = 25, a_{ii} = 6, \theta_i = 13, \tau_i = 2, \tau_z = 20, x_a = 150, x_b = 1.$) The wave is initiated at $t = 50$ by stimulating the first six excitatory cells for 5 time units and with amplitude 3. *Gray scale* shows the magnitude of the excitatory activity, which lies between 0 (*black*) and 1 (*white*). The same convention holds in all the figures of waves in the full system of equations

and $f(u) = 1/(1+\exp(-u)) \cdot u_e$, u_i are the activities of the excitatory and inhibitory populations, z is the adaptation for the excitatory populations. a_{jk} is the space-dependent connection strengths and θ_j is the space-dependent thresholds. The adaptation, $g_a(x)$ is also space-dependent. We typically use

$$K_{e,i}(x) = \frac{1}{2\sigma_{e,i}} \exp(-|x|/\sigma_{e,i})$$

as the coupling function. The functions $a_{jk}(x)$, $g_a(x)$, and $\theta_j(x)$ are generally of the form

$$r(x) = r_0 \left(1 + \frac{r_1}{1+\exp(-(x-x_a)/x_b)}\right).$$

The parameter r_0 is the baseline value, r_1 is the fractional change as x increases past x_a, the border between the two regions of excitability, and x_b controls the sharpness of the border. Numerical solutions to these equations are found by discretizing the network into 301 units for each of the u_e, u_i, z. Simulations were done using XPPAUT. Values for the parameters are given in the caption of Fig. 1.

In order to better understand the mechanisms and dynamics that underly reflected waves, we will often use a simplified model that is the normal form for the dynamics of a saddle-node on an infinite cycle; the theta model which has the following form

$$\phi_i' = 1 - \cos\phi_i - (1+\cos(\phi_i))a_0(1 + a_1 H(x - x_a)) \quad (2)$$

such that if $\phi_i = q < \pi$, then $\phi_{i\pm1} = 2\tan^{-1}(\tan(\phi_{i\pm1}) + g)$ and if $\phi_i = \pi$,then ϕ_i is reset to $-\pi$. Coupling is only via nearest neighbors. $H(x)$ is the Heaviside step function. Parameters a_0, a_1 determine the degree of excitability of the medium on either side of the border. In the following, we will justify this simplification.

3 Results

The Wilson–Cowan equations have been used successfully as a model for the spatio-temporal dynamics of cortex for many years. Each local cortical area contains a population of excitatory cells and a population of inhibitory cells. Under normal circumstances, the activity of the network is controlled by the feedback inhibition. However, in slice preparations (and in pathological situations), the inhibition is reduced and this leads to a dramatic increase in activity. Even in the

disinhibited network, the activity eventually settles down. This is due to a number of biophysical mechanisms which include spike frequency adaptation of the excitatory neurons, synaptic depression of the excitatory connections or build up of extracellular potassium. The Pinto–Ermentrout model was proposed as a simple recurrent network of excitatory cells coupled with a local negative feedback that was meant to mimic spike frequency adaptation. Thus, in this article, we use a combined model which has both spatially extended inhibition and localized spike frequency adaptation in the excitatory population. Equation 1 represents the combined spatio-temporal model.

Xu et al. found compression and reflection of evoked waves in visual cortex as the waves go from V1 to V2. They suggested that the mechanism for these phenomena was a change in the local circuit parameters as the wave progresses across the V1–V2 border. Thus, in this article, we will incorporate heterogeneities in several parameters in the model equations. There are four parameters which we allow to vary in space: a_{ee}, the excitatory–excitatory strength, θ_e, the threshold of the excitatory cells, g_a, the strength of the spike-frequency adaptation, and a_{ie}, the strength of the inhibitory to excitatory connections. Additionally, the parameters to the inhibitory neurons could also be allowed to vary, but, we do not do so in this paper. (See the results below for further justification.)

3.1 Waves in an inhomogeneous medium

We begin by showing some examples of wave propagation in the full model in which half the domain has normal values of the parameters and the other half has altered values. Figure 1 shows a typical set of simulations in which we excite a small number of excitatory cells and then plot the excitation as a function of space and time. We let the medium come to rest for 50 time units and then apply a brief (5 time units) stimulus to the first six excitatory cells. This initiates a wave of activity as seen in panel a. The velocity is uniform, as would be expected in a homogeneous excitable medium. In Fig. 1b, we increase the threshold of the excitatory cells, θ_e by 30%. This causes two clear effects. First, the wave slows down considerably, and second, the wave is compressed in both space and time. This result is consistent with the behavior observed in Xu et al. (2008) as evoked waves move from one part of the visual cortex to another. A further increase in the threshold to 51.8%, leads to the interesting phenomena of a reflected wave as seen in Fig. 1c. Here, the primary wave runs into the less excitable medium and after a pause, excites it. The lengthy pause before the right side is excited provides enough time for the left side to recover and thus be re-excited enough to produce a reflected traveling wave. There are two points worth mentioning. First the reflected wave has a slightly lower velocity than the primary wave because it is traveling into a region where the adaptation still lingers. Secondly, the wave that goes to the right has a fine periodic structure to it that is associated with the reduced velocity and higher threshold for excitation. This periodicity is not due to the discretization of the equations, but, rather, due to an instability of the smooth wave. Such waves are called "breathers" and have been found in stimulus locked traveling pulses (Folias and Bressloff 2005) and in single pulse waves (Golomb and Ermentrout 2002). If the difference in thresholds is large enough, then, propagation is blocked as shown in Fig. 1d. Thus, reflected waves appear in the boundary between transmission of the wave and block.

In Fig. 1, we changed the threshold of the excitatory cells at the midpoint of the medium. We could change other parameters as well. Figure 2a, b shows the effect of decreasing the recurrent excitatory–excitatory connection strength, a_{ee} in the right half of the medium. As was the case with the threshold change, there is compression for modest decreases in excitation and reflection for a limited range of excitation decrease. Like the change in threshold, the chance in recurrent excitation leads to a latency in firing of the right side of the medium which provides enough time for the left side to recover and produce a wave. Figure 2c, d shows the effects of increased a_{ie} the inhibitory to excitatory strength and g_a the strength of the adaptation. Neither of these changes have an appreciable effect on the velocity, and because there is no change in velocity, there can be no change in latency and thus, no reflected waves. We can easily understand why this should be so. Changes in the strength of inhibition to excitatory cells or change in adaptation affect only the *feedback* to the excitatory cells. The key to wave propagation is the ability of the medium to excite neighboring areas and, for a resting network, all that matters is the strength of excitation and the threshold which must be crossed. By the time that inhibition or adaptation take hold, the "horse is out of the barn." This observation is sufficient to also eliminate any change of the inhibitory network, such as, θ_i, a_{ii}, or a_{ei} as a mechanism for compression and or reflected waves; the main determinants of the wave velocity and latency of excitation are the strength of the excitatory–excitatory connections and the excitatory threshold.

Xu et al. pharmacologically manipulated their brain slice by adding bicuculline (BMI) which, among other things, blocks inhibition. They found that they could get rid of some of the compression and that the reflected waves disappeared. Figure 3 shows that a small change in the feedback inhibition can stop reflected waves. However, too much block of inhibition leads to run away excitation and the entire network undergoes synchronous slow oscillations (analogous to seizure behavior) with the period determined by the adaptation. BMI is not a simple drug and also has effects on potassium channels. The channels are partly responsible for setting the threshold of excitability of the neurons. Thus, we postulate

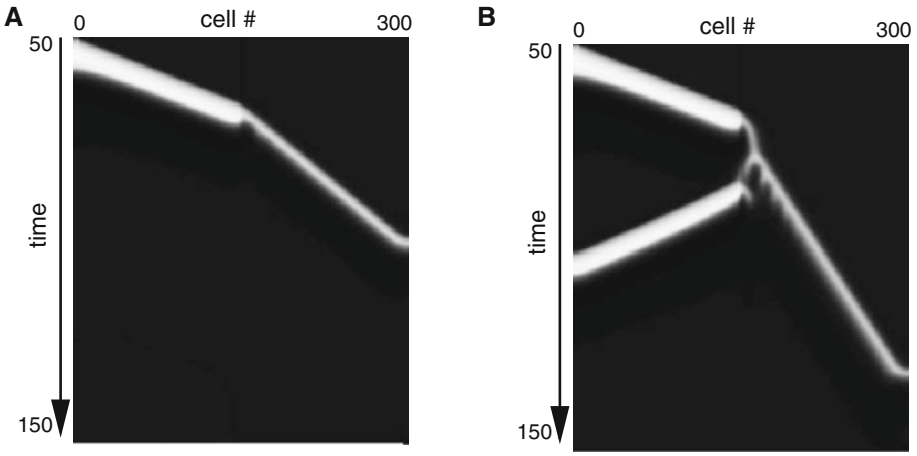

Fig. 2 Wave propagation in Eq. 1 with different types of inhomogeneities. **a** a_{ee}, the excitatory–excitatory connection strength is decreased by 25% leading to compression; **b** decrease of a_{ee} by 33.49% leads to a reflected wave; **c** increase of a_{ie}, the inhibitory to excitatory strength by 200% have no appreciable effect on the velocity; **d** increase in the strength of adaptation by 400% has no appreciable effect on velocity (parameters are as in Fig. 1)

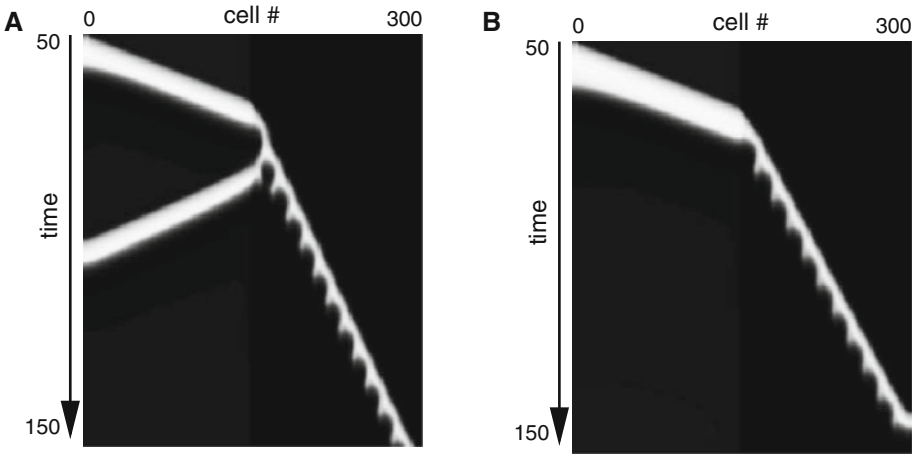

Fig. 3 Partial block of inhibition removes the reflected waves. **a** Reflected wave of Fig. 1c; **b** reduction of a_{ie} from 13 to 12 leaves compression but no reflection

that another mechanism for the effects seen by BMI are to lower the threshold of excitation. This effect could compensate for the higher threshold that we impose in Fig. 1 for the right half of the neural medium.

3.2 Quantifying the dependence on parameters

The simulations shown above illustrate how changing the degree of excitability of the medium can have a large effect on the properties of waves. For example, changes in θ_e, a_{ee} seem to affect the velocity, the width, and the magnitude of waves, while changes in the inhibitory feedback, a_{ie}, g_a change the width and magnitude but have little effect on the velocity. In this section, we quantify these features as the four parameters a_{ee}, θ_e, a_{ie}, and g_a vary. Figures 4, 5, and 6 show three measurable quantities, velocity, width, and intensity, as a function of the four parameters. As expected from the simulations of the last section, the velocity depends strongly

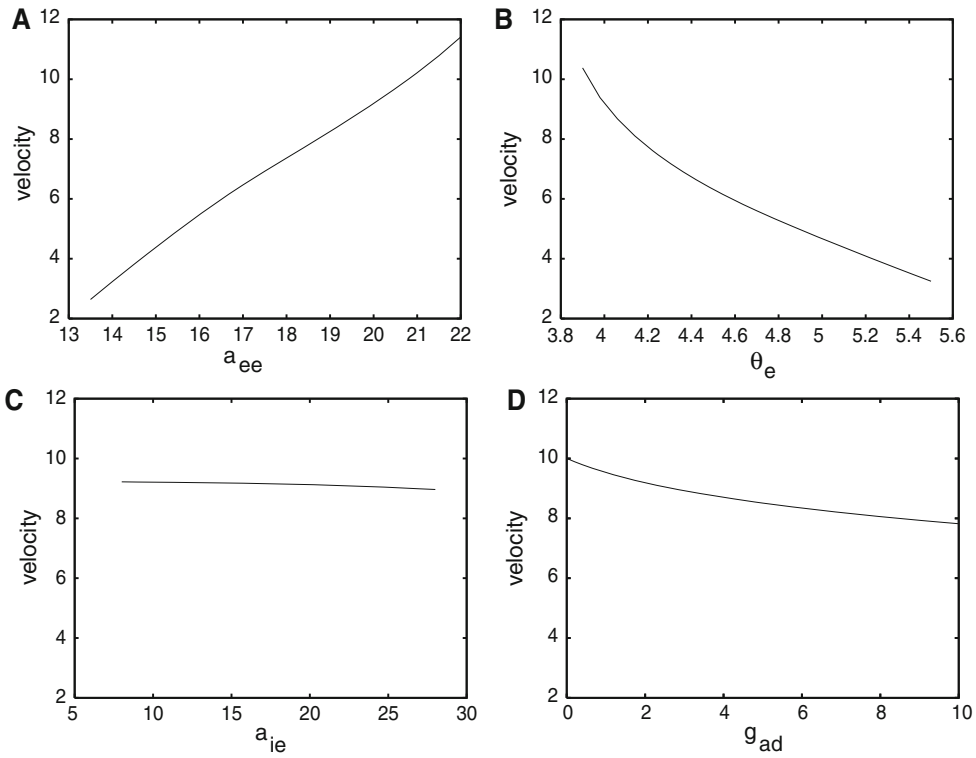

Fig. 4 Velocity of the waves as a function of the parameters in the model. **a** a_{ee}, the excitatory–excitatory coupling strength; **b** the threshold for excitation, θ_e; **c** a_{ie}, the inhibitory to excitatory coupling strength; **d** the strength of spike frequency adaptation, g_{ad}. Velocity is measured by determining the time at which cells 100 and 200 cross the $u = 0.25$ line for the first time then dividing the time difference into 100

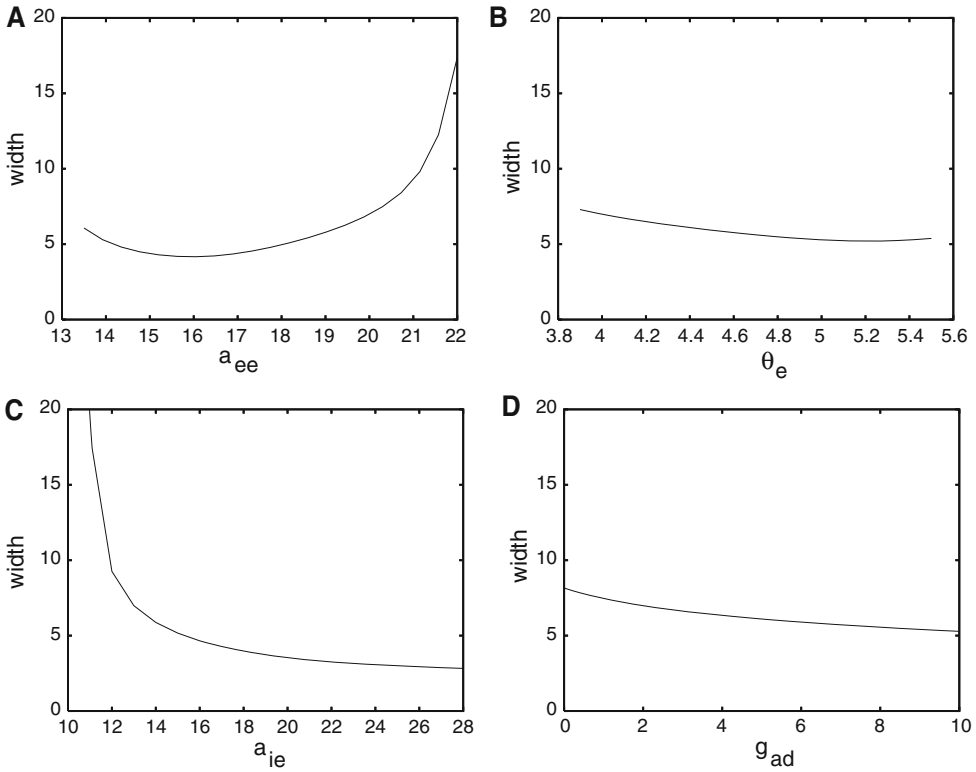

Fig. 5 Width of the waves as a function of the parameters in the model. **a** a_{ee}, the excitatory–excitatory coupling strength; **b** the threshold for excitation, θ_e; **c** a_{ie}, the inhibitory to excitatory coupling strength; **d** the strength of spike frequency adaptation, g_{ad}. Width is measured by determining the time at which cell 100 crosses $u = 0.25$ from below and then from above

on the threshold and the strength of excitatory–excitatory connections, but is almost independent of the recurrent inhibition and spike frequency adaptation. Plots a and c are completely consistent with the quantitative analysis of wave in cortical slices (Pinto et al. 2005), Fig. 6a. In this article, the authors found that the velocity was nearly independent of the concentration of picrotoxin (PTX), a blocker of inhibitory neurotransmission, but very strongly dependent on the concentration of DNQX, a blocker of synaptic excitation. In contrast, Fig. 5 shows that the width of the excitation depends

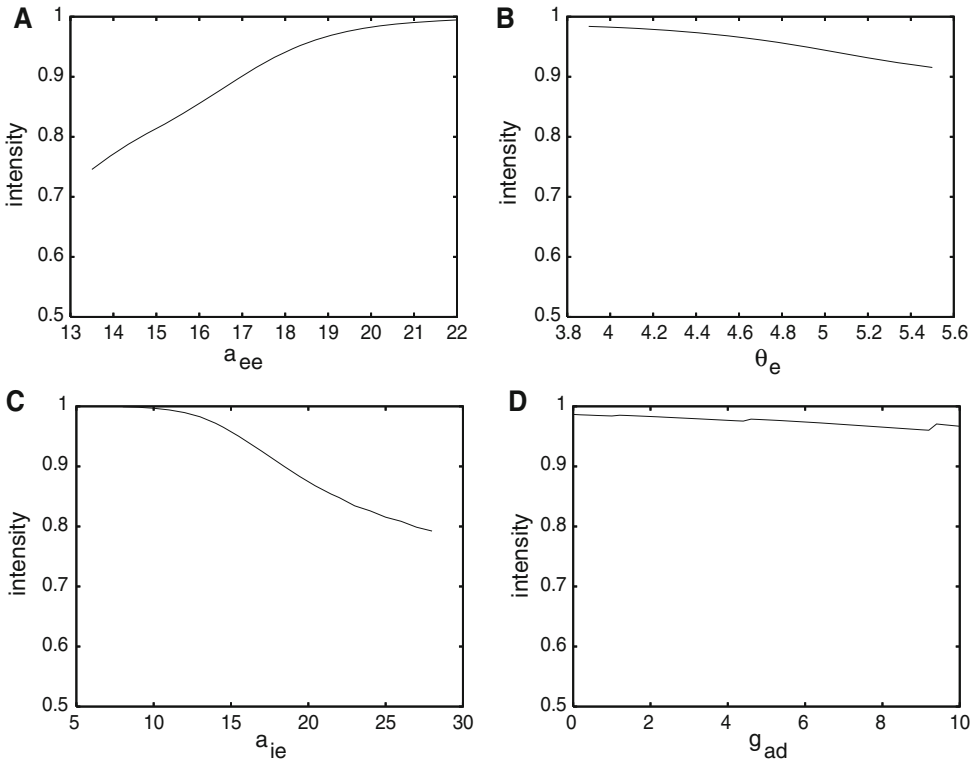

Fig. 6 Intensity of the waves as a function of the parameters in the model. **a** a_{ee}, the excitatory–excitatory coupling strength; **b** the threshold for excitation, θ_e; **c** a_{ie}, the inhibitory to excitatory coupling strength; **d** the strength of spike frequency adaptation, g_{ad}. Intensity is the maximum value of u for cell 100

strongly on both the recurrent inhibition and the recurrent excitation, but not on the threshold or the adaptation. We suspect that the weak dependence on adaptation is due to the fairly strong inhibition that is the default for our model. The strong dependence on inhibition is expected since the inhibition is the primary means of bringing the medium back to rest. Pinto et al. (2005) also measured the width of the experimental waves and found a similar strong dependence on both the excitatory and the inhibitory synaptic strength. Finally, we see that the intensity depends moderately on the synaptic excitation and inhibition. The experimental results in Pinto et al. (2005) show a decrease in intensity as synaptic excitation is reduced, but very little effect of synaptic inhibition.

The reason that the velocity is nearly independent of the synaptic inhibition and the adaptation is that, as noted above, what matters for propagation is the initial front of excitation which is independent of the delayed negative feedback. Pinto and Ermentrout (2001) exploited this idea and used singular perturbation to construct traveling waves in a network with just excitation and adaptation. Velocity in this article was completely determined by the excitation and threshold since the negative feedback was very slow.

The dependence of the width on synaptic excitation is not surprising since this excitation is required to get the wave started. The dependence on the inhibition should be reasonably clear, since inhibition (and the weaker, in this model, adaptation) is the primary way in which the network is returned to rest. For example, if we artificially slow down the inhibition, the width increases proportionally.

The intensity or amplitude would be less dependent on the inhibition if we slowed the inhibition down since slow negative feedback does not become important until the cells have made their transition to the excited state, which, is, up to saturation, dependent on the recurrent excitation.

3.3 Simplified models for reflection and compression

We now turn our attention to the mechanisms for reflection and compression of waves. We believe that compression is nothing more than a visible signal of reduced velocity in the medium and some modest change in the width of the waves. To better understand the underlying dynamics of reflection, we first look at the space-clamped system:

$$\begin{aligned} \frac{du_e}{dt} &= -u_e + f(a_{ee}u_e - a_{ie}u_i - g_a z - \theta_e) \\ \tau_i \frac{du_i}{dt} &= -u_i + f(a_{ei}u_e - a_{ii}u_i - \theta_i) \\ \tau_a \frac{dz}{dt} &= -z + u. \end{aligned} \tag{3}$$

Since the primary variable that we altered to obtain reflected waves is the excitatory threshold, θ_e, we will treat that as a bifurcation parameter. Figure 7a shows the behavior of the system as a function of the parameter θ_e. For θ_e larger than 3.83 (shown by the arrow in the figure), the only stable state is

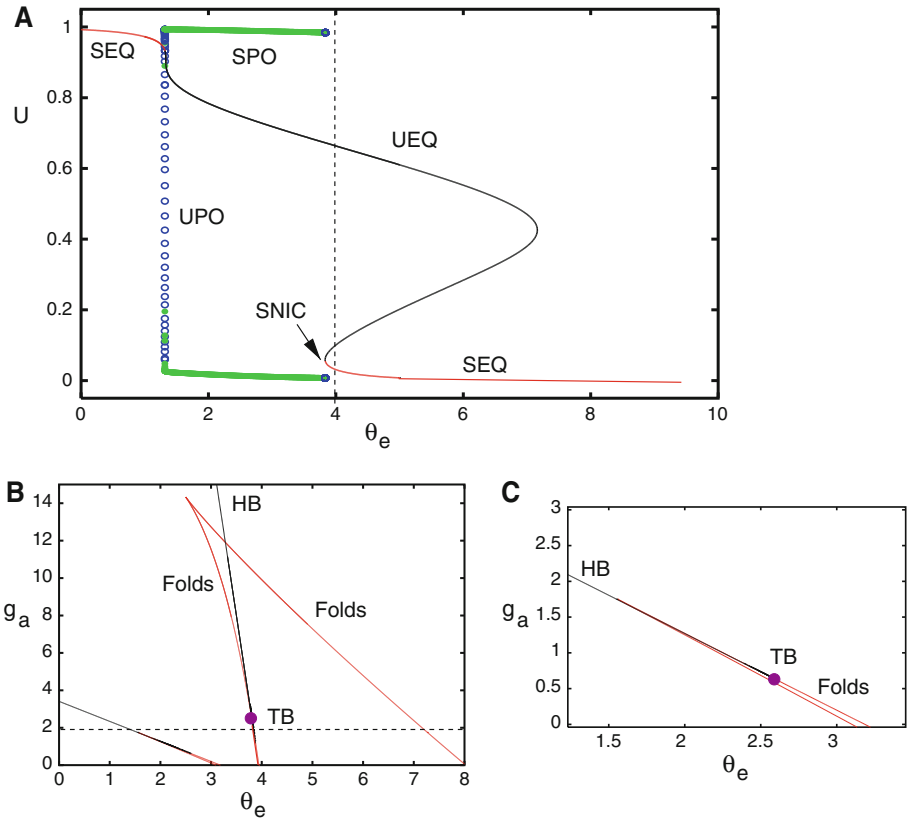

Fig. 7 Bifurcation diagram for the space-clamped system (3) as the threshold, θ_e varies. **a** One parameter diagram. Stable equilibria (SEQ) (maxima and minima of u are shown) are in *red* and unstable (UEQ) in *black*. *Filled green circles* are stable periodic orbits (SPO) and *hollow blue circles* are unstable periodic orbits (UPO). The saddle-node infinite cycle (SNIC) is shown. **b**, **c** Two parameter diagram with g_a as the other parameter. Red curves represent fold bifurcations and *black* are curves of Hopf bifurcations (HB). The *right figure* is just an expanded view of the left. *Filled circles* represent Takens–Bogdanov (TB) points

the resting equilibrium (bottom right, labeled SEQ). For very low threshold, there is a stable excited state (red curve at the top left, SEQ) which becomes unstable via a Hopf bifurcation and a nearby fold bifurcation. The periodic branch of solutions emerging from the Hopf point is unstable (labeled UPO) but "turns around" to form a large amplitude branch of periodic orbits (solid green circles, SPO). This branch persists as θ_e increases until it hits the saddle-node point at $\theta_e \approx 0.383$, a saddle-node infinite cycle (SNIC) bifurcation. Figure 7b, c shows that the fold point persists as g_a changes but that the lower branch can lose stability at a Hopf bifurcation for g_a large enough. The filled circle shows that the transition from a fold to a Hopf on the lower branch occurs via a Takens–Bogdanov bifurcation where the branch of Hopf bifurcations (HB) hits the branch of folds.

The main point of the bifurcation analysis is to show that underlying the excitability of the waves is a SNIC bifurcation. The SNIC is a well-studied system and has a very simple reduced representation called the "theta model" (Ermentrout and Kopell 1986). It is possible to formally reduce the full model, Eq. 1 to a scalar integro-differential equation model if we assume that the system is poised near the SNIC bifurcation. Rather than do this explicitly, we will just write down two equivalent versions of the dynamics near the onset of the bifurcation. Near the saddle-node, the dynamics is characterized by the very simple quadratic differential equation

$$\frac{dv}{dt} = v^2 + b.$$

For $b = -a^2 < 0$, the system has two equilibrium points, $v = -a$, a stable rest state, and $v = a$, an unstable equilibrium. Initial conditions such that $v(0) > a$, will rapidly grow to infinity in a finite amount of time, in which case we say that system has fired. When v hits $+\infty$, it is reset to $-\infty$, where it returns to $-a$, the resting state. If we allow a to be space-dependent, and assume spatially decaying coupling, we obtain

$$\frac{\partial v(x,t)}{\partial t} = v(x,t)^2 - a(x)^2 + \int_{-\infty}^{\infty} K(x-y)P(v(y,t))\,dy, \tag{4}$$

where $K(x)$ is an effective coupling kernel (a combination of K_e and K_i) and $P(v)$ is a measure of the excitation. For example, P may be close to zero except for values of v near q where $a < q \leq \infty$. We call q the spike threshold. If $K(x) \geq 0$, then, we expect that if a group of neurons is excited past $v = a$, then, they will cross $v = q$ and provide enough excitation to move a cell at $v = -a$ past $v = +a$ and thus create a wave of excitation. For the purposes of numerical simulation, it is easier to convert Eq. 4 to a theta model by making the transformation, $v(x,t) = \tan\phi(x,t)/2$.

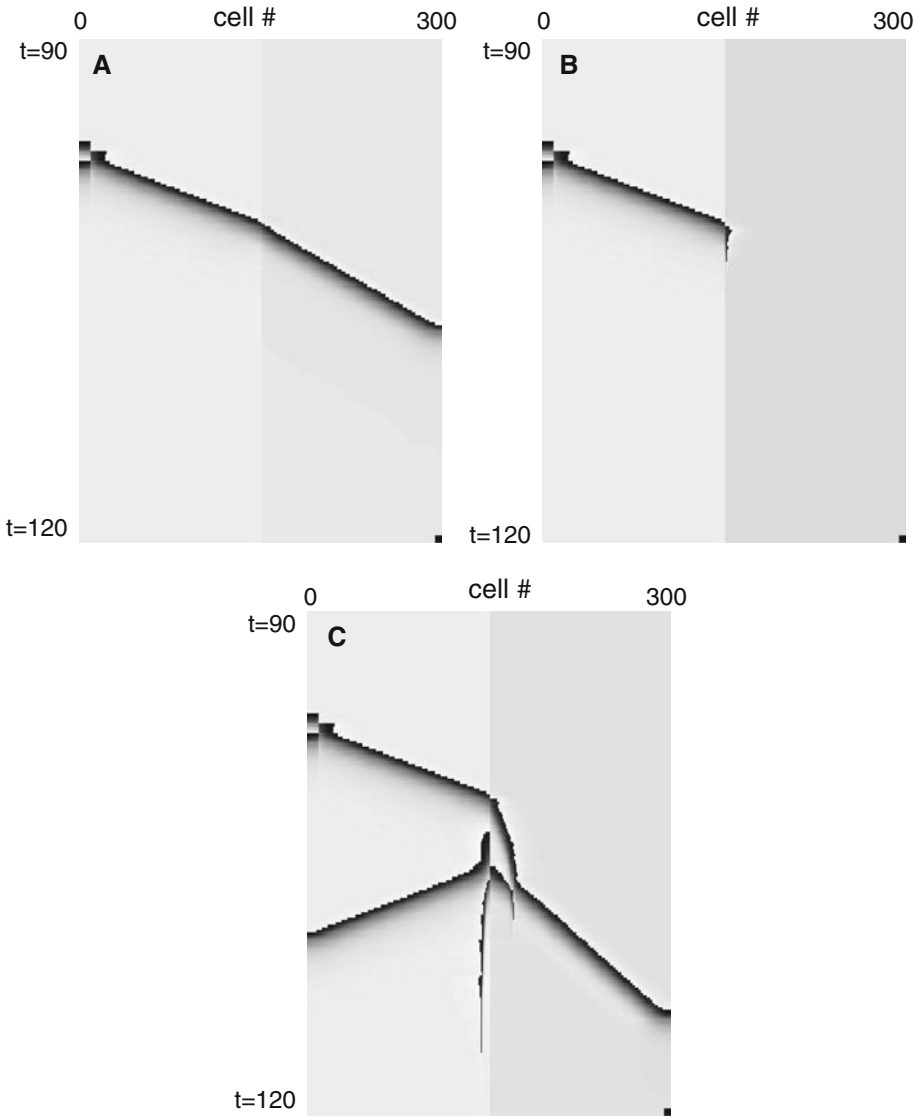

Fig. 8 Numerical solution to the theta model, Eq. 5 for $K(x) = 2.5\exp(-|x|/10)$, $P(\phi) = \exp(-120(1-\cos(\phi-2)))$, and $a(x)^2 = 0.05$ for $x < 150$ and **a** $a(x)^2 = 0.1$ for $x \geq 150$; **b** $a(x)^2 = 0, 3$ for $x \geq 150$; and **c** $a(x)^2 = 0.3$ for $x \geq 150$

(As $\theta_{e,i}$ are thresholds for the full model, we use ϕ here instead of the traditional θ.) With this transformation, Eq. 4 becomes

$$\frac{\partial\phi(x,t)}{\partial t} = (1-\cos\phi(x,t)) + (1+\cos\phi(x,t))\left[-a(x)^2 + \int_{-\infty}^{\infty} K(x-y)P(\phi(y,t))\,\mathrm{d}y\right]. \quad (5)$$

We are now free to define P, however, we like. Osan et al. (2002) proved that there were traveling wave solutions to (5) when P represented a time-dependent synapse. They also showed that if the spike threshold, $v = q$ is set to the natural value of $q = \infty$ (corresponding to $\phi = \pi$), the medium will always recover enough so that successive neurons firing will induce neurons that have already fired to fire again. Thus means that the network will never come to rest. The reason for this pathology is setting the spike threshold exactly at $+\infty$ makes the recovery period too short. Thus, we will always let $q \in (a, \infty)$.

Figure 8 shows a space–time plot for a numerical simulation of (5) with the functions $K(x)$, $P(\phi)$ given in the caption. As with the full three variable model, we get compression (a slowing down) of the wave as the threshold a increases. If this threshold is too large, then block occurs as illustrated in Fig. 8b. Finally, for an intermediate value for threshold, there is a reflected wave (panel c).

3.3.1 Phase plane analysis of reflected waves

Ermentrout and Rinzel (1996) presented a simple phase-plane analysis of a pair of diffusively coupled phase models and showed that reflected waves could be explained by proving that there was an unstable periodic solution. Diffusive or gap junctional coupling acts for all values of the oscillator, while pulse coupling as we have here is active

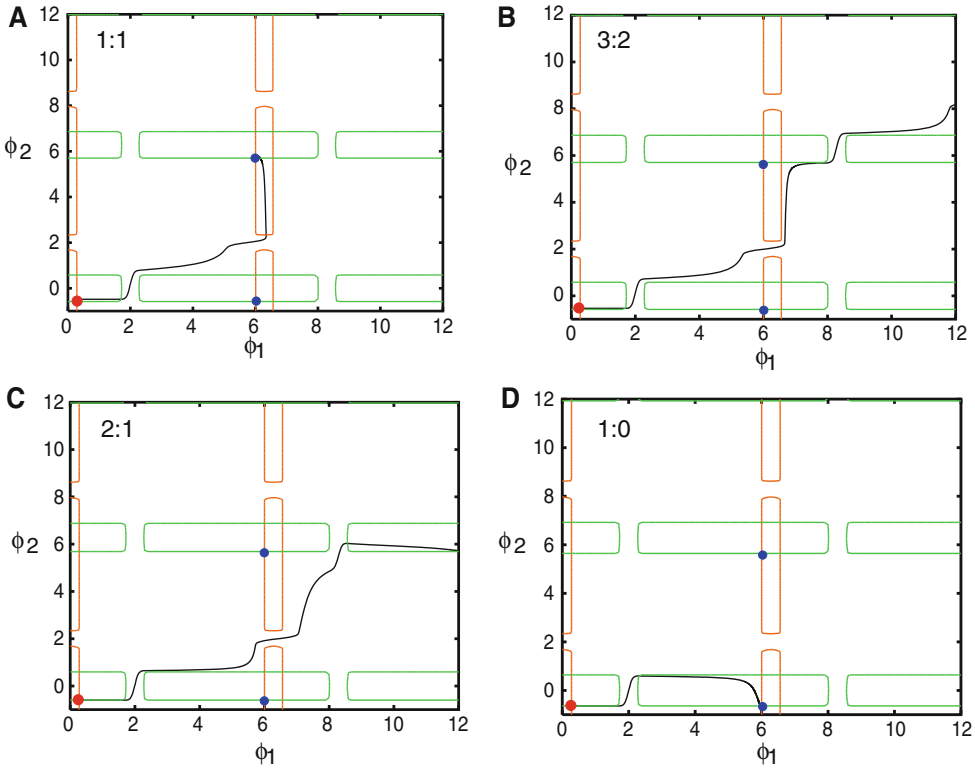

Fig. 9 Phase plane for Eq. 6, a simple two oscillator model for reflected waves. $P(\phi) = \exp(-120(1-\cos(\phi - 2)))$, $g = 4$, $a_1 = 0.02$ and a_2 varies. Plots show the nullclines (ϕ_1 nullcline in *red* and ϕ_2 nullcline in *green*) and the unstable manifolds of the saddle point shown by the *red filled circle*. *Blue filled circles* show the stable fixed points. **a** 1:1, normal propagation, $a_2 = 0.06$; **b** 3:2 cycle $a_2 = 0.075$; **c** 2:1, reflected wave, $a_2 = 0.095$; **d** block, $a_2 = 0.11$

only in a limited range of active phases. Thus, the mechanisms for reflected waves in this model and the model presented in Ermentrout and Rinzel (1996) may be different. For completeness, we offer a simple phase plane analysis for the pulse-coupled system:

$$\dot{\phi}_1 = 1 - \cos\phi_1 + (1+\cos\phi_1)[-a_1 + gP(\phi_2)] \qquad (6)$$
$$\dot{\phi}_2 = 1 - \cos\phi_2 + (1+\cos\phi_2)[-a_2 + gP(\phi_1)]$$

where $a_1 = 0.02$ and $a_2 > a_1$ varies. $P(\phi)$ is as defined above. We start each neuron at its rest point and then initialize ϕ_1 to be slightly above threshold. This causes ϕ_1 to "fire" and then induce ϕ_2 to fire.

Figure 9 shows the phase plane for this system. The threshold for firing of ϕ_1 is determined by a saddle point which is shown in the figure by the large red circle. Trajectories that start near this point are rapidly attracted to the unstable manifold for the saddle so this is what we plot as the parameter a_2 varies. Large a_2 means that ϕ_2 is very inexcitable and requires a large kick to stimulate it. Each panel shows the nullclines; the wide (tall) rectangular plots are the ϕ_2 (ϕ_1) nullclines in green (orange). Blue filled circles show the stable fixed points. Panel a ($a_2 = .06$) shows a case in which each neuron fires once. This is the analogue of successful propagation of the wave through the medium. Panel d ($a_2 = 0.11$) shows an example of block in which only ϕ_1 completes a firing cycle. We can see what has happened. Since the initial value of ϕ_2 (which is the resting state of ϕ_2) is lower for larger values of a_2, the unstable manifold starts out nearly along this rest state (since $P(\phi_1)$ is essentially zero until ϕ_1 gets large enough). Once ϕ_1 does get large enough, ϕ_2 can escape from the rest state and starts to increase. If it moves upward enough as in panel a, it can escape and increase by 2π (that is, "fire"). In panel d, we see that by the time ϕ_1 has moved out of the region where $P(\phi_1)$ is nonzero, ϕ_2 has not increased enough and is trapped by its nullcline and collapses back to rest. We also see that in panel a, ϕ_2 increased fast enough so that ϕ_1 crosses into its nullcline (tall orange rectangle) and returns to a rest state, However, in panel c ($a_2 = 0.095$), while ϕ_2 escapes its nullcline, it does so just barely, and thus ϕ_1 has increased quite a bit before ϕ_2 starts its rapid rise. Thus, ϕ_1 escapes the trap of its nullcline and can then fire again before coming to rest when ϕ_2 is caught by its (green) nullcline. Thus, ϕ_2 has completed one cycle but ϕ_1 has completed two; this is the analogue of a reflected wave. Further decreases in a_2 allow ϕ_2 to escape its nullcline and fire again. Panel b shows an example where ϕ_2 fires twice and ϕ_1 fires three times. As we change a_2 either ϕ_1 gets trapped by its (orange) nullcline and there is m:m echo (each neuron fires m times) or ϕ_2 gets caught by its (green) nullcline and there is $m+1$:m echo (ϕ_1 fires $m+1$ times and ϕ_2 fires m times).

3.3.2 Nearest neighbor with map

As our final analysis of reflected waves in a synaptically connected network, we consider a discrete space model with only nearest neighbor coupling:

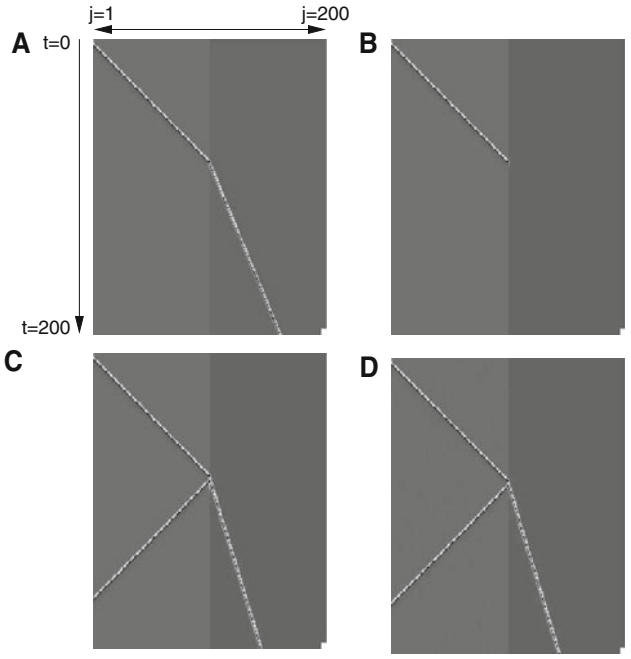

Fig. 10 Waves in a chain of theta neurons with nearest-neighbor connectivity. There are 200 units in the chain; $\alpha_j = 0.25$ for $1 \geq j < 100$ and $\alpha_j = 0.25 + c$ for $100 \leq j \leq 200$. $\phi_T = 2$, $g = 1.3$. **a** Compressed wave, $c = 0.14$; **b** wave block, $c = 0.18$; **c** reflected wave, $c = 0.16$; **d** reflected wave with noise added to the medium, $c = 0.16$

$$\phi_j' = 1 - \cos(\phi_j) - \alpha_j(1 + \cos(\phi_j)).$$

Coupling is through nearest neighbors and takes the following form (see Hoppensteadt and Izhikevich 1997): when ϕ_j crosses ϕ_T, then $\phi_{j\pm1}$ are set to

$$2 \arctan\left[\tan(\phi_{j\pm1}/2) + g\right]$$

where g is the coupling strength. The parameters, α_j determine the degree of excitability; larger values of α_j correspond to less excitable media. In the simple chain model, we set α_j to be a^2 for $j = 1, \ldots, N/2$ and to be $b^2 = a^2 + c$ for $N \geq j > N/2$. The parameter c describes the heterogeneity. Figure 10 shows the results of a numerical simulation of the chain. If c is small enough, a single wave propagates through but slows down once the less excitable medium is reached. This corresponds to compression of the waves and is shown in panel a. In Fig 10b, c is too large and the medium fails to become excited on the right. If c is an intermediate value, then, there is a reflected wave as shown in Fig. 10c. Panel d shows that the reflected waves are robust in the presence of noise. Thus, the chain behaves in a way very similar to our previous models. We proceed to obtain bounds on c for which we can expect to find reflected waves. In order to facilitate the analysis, we consider the untransformed theta model which is the quadratic integrate and fire model with infinite reset:

$$V_j' = V_j^2 - a_j^2 + g\left[\delta(t - t_{j-1}) + \delta(t - t_{j+1})\right] \tag{7}$$

where V_j is the "voltage", t_j are the times that the jth unit crosses $0 < q \leq \infty$. We call $V_j = q$ the synaptic threshold since when this is crossed, communication between the two cells occurs. The theta model is defined in such a way that $V_j = \tan(\phi_j/2)$, so that $q = \tan(\phi_T/2)$. We see that $a_j = \sqrt{\alpha_j}$ with regard to the simulations in Fig. 10. We work on the bi-infinite chain, $-\infty < j < \infty$ with $a_j = a$ for $j < 0$ and $a_j = b$ for $j \geq 0$. Thus, the medium changes its excitability at $j = 0$. Since the coupling is limited to the nearest neighbor, all that matters is when an adjacent cell fires. As $V_j = -a_j$ is a stable rest state, we assume the network is initially at rest and induce a wave by exciting a single unit. We will always assume the following strict requirement: $g - a_j < q$. This condition is required as it guarantees that a stimulus will not cause a cell to immediately cross the synaptic threshold. Were this the case, then propagation speed would be infinite, a nonphysical situation. (Such a scenario could be rectified by incorporating a delay in the coupling.) We consider two adjacent units with $a_j = a,\ b$, respectively; we could have $b = a$. As our focus is on reflected waves and compression, we will have $b \geq a$ in general. We will also call these adjacent units a and b, respectively. Since we have manipulated the excitability in our simulations, we do the same thing here and treat b as our main parameter. (With regard to the simulations in Fig. 10, $b = \sqrt{\alpha + c}$ and $a = \sqrt{\alpha}$.) At $t = 0$ unit a fires, that is $V_a = q$ and since unit b is at rest it will be instantly incremented to $V_b = -b + g$. If $-b + g < b$, then unit b fails to fire and we obtain propagation failure. Thus, the maximum value that b can take is $g/2$, that is, to assure propagation, $b < g/2$. The velocity of the wave is simply the inverse of the time it takes to get from $-b + g$ to synaptic threshold, q, that is

$$\tau_{bq} := \int_{-b+g}^{q} \frac{\mathrm{d}x}{x^2 - b^2} = \frac{1}{2b} \ln \frac{g(q-b)}{(q+b)(g-2b)}.$$

Since $q > b$ and $g > 2b$, this time is finite and positive. We can define τ_{aq} analogously. τ_{bq} is a monotonically increasing function of b. This follows since τ_{bq} is the time it takes to go from $V = -b + g$ to $V = q$ where $V' = V^2 - b^2$. By assumption $-b + g > b$ so $V' > 0$. Let $V_1' = V_1^2 - b_1^2$ and $V_1' = V_2^2 - b_2^2\, b_1 < b_2$, with $V_1(0) = g - b_1$ and $V_2(0) = g - b_2$. Suppose $b_1 < b_2$. Then $V_1' > V_2'$ and $V_1(0) > V_2(0)$. Thus, $V_1(t) > V_2(t)$, so that V_1 will cross q first and thus, τ_{bq} is monotonically increasing with b. From this, we immediately see compression of the wave since the waves to the right are slower than those to the left when $a < b$. What is needed to get or prevent reflection? Once unit a has fired, it will evolve back toward rest by first blowing up to $+\infty$ and then moving from $-\infty$ toward, $-a$. When unit b fires, unit a will be incremented by an amount g. This will induce unit a to fire only if $V_a(t) + g > a$ and otherwise, unit a will not fire. The latter case means we get regular

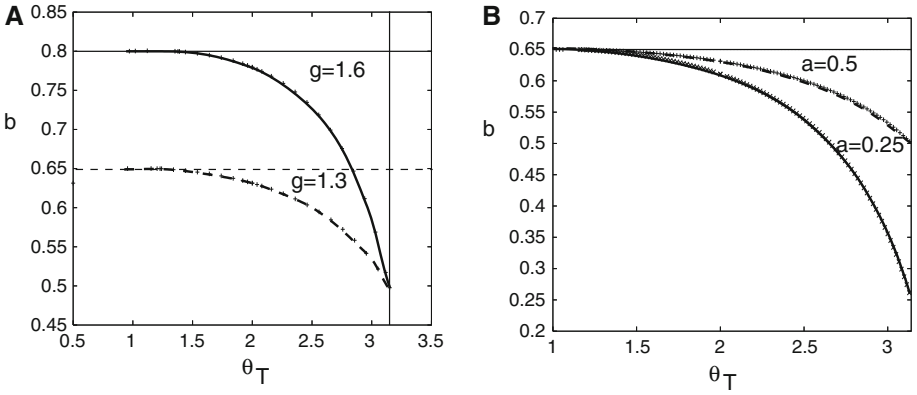

Fig. 11 Range of excitability, b of the right half of the medium as a function of synaptic threshold such that there will be reflected waves. Above the *horizontal lines* leads to block and below the *curved lines* leads to normal propagation. Region denoted RW leads to reflected waves or more complex dynamics. **a** Effects of the coupling strength, g; ($a = 0.5$). **b** Effects of the excitability of the *left side*, a ($g = 1.3$)

propagation and the medium fires a single wave with compression on the right. We define

$$\tau_{a,\max} := \int_q^{\infty} \frac{\mathrm{d}x}{x^2-a^2} + \int_{-\infty}^{a-g} \frac{\mathrm{d}x}{x^2-a^2} = \frac{1}{2a} \ln \frac{g(q+a)}{(q-a)(g-2a)}.$$

This expression is the maximum amount of time allowed between the time that unit a crosses synaptic threshold, q and unit b crosses q in order to guarantee that unit a does not again fire. Thus, we will get regular propagation and no re-excitation of the medium if $b < g/2$ and $\tau_{bq} < \tau_{a,\max}$:

$$\frac{1}{2a} \ln \frac{g(q+a)}{(q-a)(g-2a)} > \frac{1}{2b} \ln \frac{g(q-b)}{(q+b)(g-2b)}. \tag{8}$$

Since cells to the left of unit a (which is on the border of the excitability change) have recovered even more if unit a fires again, then we will always get a wave propagating to the left, a reflected wave. Let us examine Eq. 8 in more detail. Let $b = a$; that is to assume a perfectly homogeneous medium. Does this inequality hold? If not, then there will not even be a legitimate traveling wave that generates only one bout of excitation. Our model is symmetric about $V = 0$, so that the time it takes to go from $g - a$ to q is exactly the same as the amount of time it takes to go from $-q$ to $a - g$. Similarly, the amount of time to go from $-\infty$ to $-q$ is the same as to go from q to $+\infty$. Thus,

$$\tau_{a,\max} = 2 \int_q^{\infty} + \tau_{aq}.$$

This guarantees that as long as $q < \infty$, there can be a regular traveling wave in a homogeneous medium. If $q \to \infty$, then $\tau_{a,\max} = \tau_{aq} < \tau_{bq}$ if $b > a$, even the smallest inhomogeneity will induce re-excitation and pathological firing. It is for this reason that in both the theta model with continuous coupling simulated earlier, and the present model, that we require the synaptic threshold to be finite (or, in the theta model, to be less than π). Equation 8 provides a way to estimate boundaries for which there is repeated activity. Given, for example, a, q, g, we can find a range for b such that there will be reflected waves. Reflected waves, or, more precisely, waves which re-excite the left-hand side at least one time, occur when $b_{\min} < b < g/2$ where $b_{\min}$ is defined by $\tau_{a,\max} = \tau_{b_{\min} q}$. We have already shown that as long as $q < \infty$, $\tau_{a,\max} > \tau_{aq}$ and we know that $\tau_{bq} \geq \tau_{aq}$ with equality for $b = a$ and τ_{bq} is a monotonically increasing function of b that approaches $+\infty$ as $b \uparrow g/2$. Thus, there is a unique root, $b_{\min}$, to $\tau_{bq} = \tau_{a,\max}$ with $a < b_{\min} < g/2$. Reflected waves will occur for b in some range greater than a and less than $g/2$ for all finite values of q. We can apply these calculations to Fig. 10 where $g = 1.3$, $a = \sqrt{\alpha} = 0.5$, and $q = \tan 1 \approx 1.5574$. We find that $\tau_{a,\max} \approx 2.13196$ and, numerically solving for $b_{\min}$, we get $b_{\min} \approx 0.63137$. In terms α and c, we expect to get reflected waves for $b_{\min}^2 - \alpha < c < g^2/4 - \alpha$ which leads to $0.1486 < c < 0.1725$. Figure 10 confirms these bounds.

Figure 11 shows the ranges of excitability, b such that there will be reflected waves as the synaptic threshold, ϕ_T (or alternatively, $q = \tan(\phi_T/2)$) varies. Reflected activity will occur for b between the upper horizontal line and the lower curved line. Above the horizontal line, there is wave block and below it, there is normal propagation. In the left panel, we show how the coupling strength alters the window of excitability. In general, the stronger the coupling, the larger the window. Note that as ϕ_T approaches π, the window extends from $g/2$ to a. As we saw above, it is impossible to get normal waves passing through the medium without reflection of $q = +\infty$ or $\phi_T - \pi$. The right-hand figure shows a similar plot where the excitability of the left-hand medium is increased (a goes from 0.5 to 0.25). Again, the window is wider; it is much easier to get reflected waves when the medium is very excitable (recall $a = 0$ is the transition to spontaneously oscillatory activity). So far, we have shown that if b is too large there will be wave failure, for b small enough, there will be normal propagation but with compression, and for intermediate values of b, re-excitation is possible. Re-excitation, however, does not imply that the waves are as depicted in Fig. 10c, d. To guarantee exactly one reflected wave, we need to make

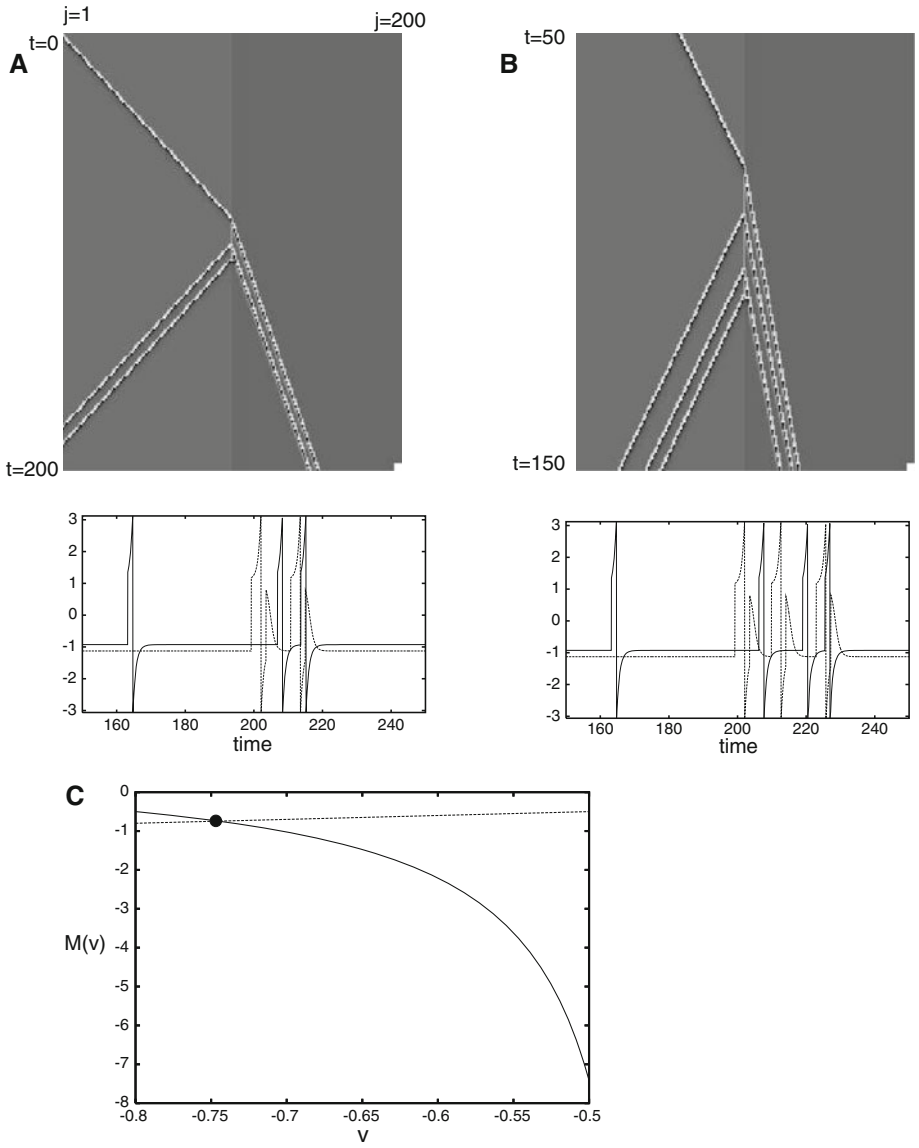

Fig. 12 Complex reflected waves. **a**, **b** Space–time plots (*top*) and $\phi_{80}(t)$ (*solid*) and $\phi_{120}(t)$ (*dashed*) (*bottom*) $a = 0.5$, $q = \tan(1)$, $g = 1.3$, $b = \sqrt{.25 + c}$. **a** $c = 0.148635$; **b** $c = 0.1486382$. **c** Map establishing the existence of an unstable periodic orbit for the heterogeneous medium

sure that the right-hand side does not get re-ignited, once the left-hand side initiates a reflected wave. Near the lower value, $b_{\min}$, V_a just barely makes it past a so that it can take a long time for the left-hand side to initiate a reflected wave. This means that the right-hand side gets closer to rest so that when the reflected wave is initiated, a new wave could occur on the right. Thus, we expect that there should be a complex sequence of waves near $b = b_{\min}$. This phenomena was seen and explained in Ermentrout and Rinzel (1996) for gap-junction coupled excitable systems.

Figure 12a, b shows two examples of complex reflected waves producing two reflected waves and two waves back into the right-hand medium. As the parameter c (which is the increase in excitability) changes, more and more complex waves appear to emerge. A suggested mechanism for this complexity was given in Ermentrout and Rinzel (1996) in which the authors suggested the existence of an unstable periodic orbit which alternately produces waves emanating from the middle of the medium. In that paper, the authors considered a diffusively coupled medium with heterogeneities and then looked at a simple pair of coupled cells. Using phase-plane techniques, they proved the existence of an unstable periodic orbit. If initial data are close to this periodic orbit, then a number of transient circuits are made before returning to rest. These transients correspond to reflected waves in the full system. More recently, Cytrynbaum and Lewis (2009) numerically showed that there was an unstable periodic orbit in a one-dimensional homogeneous diffusively coupled excitable medium. With carefully tuned initial data, they are able to evoke a transient set of pulses emitted from the middle of the medium. In our situation, we cannot control the initial data as the medium is excited by a stimulus at

one end. However, if the unstable periodic orbit persists for the heterogeneous medium (and it will if the heterogeneity is not too big), then we can manipulate how close the incoming externally evoked wave gets to the unstable periodic orbit and thus create reflected waves such as those seen in Fig. 12a, b. The simple diffusively coupled two-cell model in Ermentrout and Rinzel (1996) required qualitative phase plane methods for analysis since explicit solutions were not available. However, in our pulse-coupled system, it is quite straight forward to find an unstable periodic orbit for the two-cell system. Rather than show this for the heterogeneous system, we show an unstable periodic orbit for the homogeneous system as the calculation is very easy. Since the orbit is unstable, it is structurally stable so that if the parameters are changed, the unstable periodic orbit will persist up to a point. This means it also exists for the heterogeneous medium. Thus, consider the two-cell model, $\mathrm{d}V_j/\mathrm{d}t = V_j^2 - a^2$ for $j = 1, 2$. Suppose $V_1 = q$ and $V_2 = u < -a$. V_2 will be incremented to $u + g < q$. V_1 will go to $+\infty$, be reset to $-\infty$ and gradually tend toward $-a$. In the meantime, V_2 will increase until it reaches q. At this point, $V_1 = u'$ and we are exactly in the reverse situation that we started with. The map from u to u' is our Poincare map and fixed points will correspond to periodic orbits. Using the formulae above, we see that

$$\int_{g+u}^{q} \frac{\mathrm{d}x}{x^2 - a^2} = \int_{q}^{\infty} \frac{\mathrm{d}x}{x^2 - a^2} + \int_{-\infty}^{u'} \frac{\mathrm{d}x}{x^2 - a^2}. \tag{9}$$

That is, the time from V_2 to go from $u + g$ to q is the time it takes from V_1 to go from q to ∞ and $-\infty$ to u'. As these integrals can be easily evaluated, we can write an exact map for u' as a function of u:

$$u' = M(u) := -\frac{(a^2 + q^2)(u + g) - 2qa^2}{a^2 + q^2 - 2q(g + u)}.$$

Before analyzing this map, we remark that if the medium is heterogeneous, the maps will not be so simple since we will not be able to get rid of the logarithms; little insight will be gained. This map is not valid for all u. Indeed, it is predicated on several assumptions: $u < -a$ and $q > u + g > a$. Fixed points of the map are solutions to a quadratic equation, $u = M(u)$; the relevant fixed point is

$$u_0 = -\frac{1}{2q}\left(gq - (a^2 + q^2) + \sqrt{(a^2 - q^2)^2 + q^2 g^2}\right)$$

and the derivative of the map at u_0 is

$$M'(u_0) = -\left(\frac{q^2 - a^2}{-gq + \sqrt{(a^2 - q^2)^2 + q^2 g^2}}\right)^2.$$

Neither of these expressions are particularly enlightening, however, we can approximate them for large q (since we do want q large enough) as

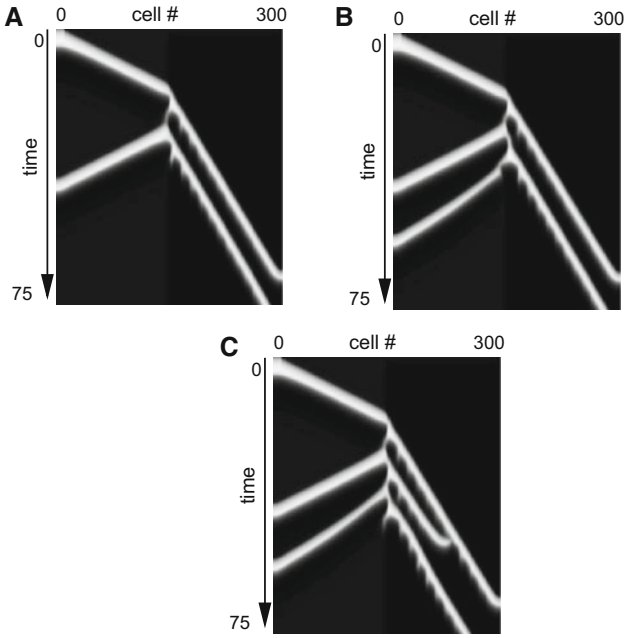

Fig. 13 Exotic waves in Eq. 1. As it is easier to get exotic waves when there is no adaptation, we set $g_a = 0$ and to compensate, set $a_{ie} = 15$. For these simulations, we increase the threshold of the excitatory cells by different percentages for each panel and also increase the inhibitory threshold by 50%. **a** 2:2 waves (41.5%); **b** 3:2 waves (41.04%); **c** 3:3 waves (41.2%)

$$u_0 \sim -\frac{g}{2} + \frac{a^2 - g^2/4}{q} + \ldots$$
$$M'(u_0) \sim -1 - \frac{2g}{q} + \ldots.$$

Since $g > 0$, this implies that $M'(u_0) < -1$ so that the fixed point is unstable and thus there is an unstable periodic orbit for q large enough. For the choice of parameters in the figures, $g = 1.3, q = \tan(1), a = 0.5$, we find $u_0 = -0.745$ and $M'(u_0) = -5.27$, thus there is an unstable periodic orbit. The map is illustrated for these values in Fig. 12c. While this calculation does not prove the existence of an unstable periodic orbit for the full chain, it provides an argument as to why such an orbit should exist.

3.3.3 Complex waves in the full model

The arguments above for both the discrete chain and the pair of coupled neurons argue that the possibility of complex patterns of activation should occur generically for a heterogeneous medium. Thus, we go back to the full model, Eq. 1 and see if we can find any complex waves by adjusting, say, the threshold in the right-hand side of the medium. In Fig. 13, we illustrate several examples of complex reflected waves in the full Eq. 1. Here, in order to make it easier to find the waves, we have removed the spike frequency adaptation and also increased the threshold for inhibition in the right

half of the medium. These waves can be found in our "standard" model, but require adjusting parameters to many decimal places rather than just three in the present case. As these waves occur in very narrow parameter regimes, it is not likely that they would be readily observed.

4 Discussion and conclusion

The main result of this article is to show that compression and reflection of waves in homogeneous cortical networks could be simply due to a loss of excitability of the medium into which the wave travels. Indeed, too little excitability prevents propagation altogether. Simple and complex reflected waves occur in the boundary between normal propagation and block. We have shown how the velocity of waves depends on several parameters, notably, the threshold for the excitatory waves, the strength of excitatory–excitatory conductances, the degree of spike frequency adaptation, and the amount of feedback inhibition. The latter two are important factors in preventing run-away excitation of the network. However, they have little effect on the intrinsic excitability of the medium due to the fact that they only come into play after the excitatory cells become active. As the adaptation and the inhibition are important in controlling activity, they have a major effect on the width of the wave. That is, the inhibition controls both the spatial extent of the region of excitation and how long it persists. Our simulations are consistent with the experimental measurements of Pinto et al. (2005) which showed little dependence of the velocity on the inhibition but a strong dependence on the wave duration. We also propose that keeping the threshold low on the right half of the medium would reduce the compression and eliminate the reflected waves. This hypothesis could be tested by using more specific drugs such as gabazine (for blocking inhibition) or a specific potassium channel blocker. That is, we would predict that gabazine would not have a big effect on compression and reflection, but the potassium channel blocker would.

In this study, we focus on the dynamics of type I neurons. Previous studies found it difficult to get reflection in a network of type II neurons, see for instance Ermentrout and Rinzel (1996). We have also tried to get reflection in type II networks for this system, but we were not successful. In a recent paper, Ozeki et al. (2009) suggested that, in V1, the nullclines intersect in the middle branch of the excitatory nullcline. This fixed point is stabilized from strong recurrent inhibition. In our system, it can also be stabilized, but only if the inhibition is very fast compared to the excitation. However, if the inhibition is very fast, waves are prevented. One can thus regard our requirement for type I excitability as a prediction about the state of the cortex.

In order to explain reflected waves, we first studied a simple two-dimensional model and used the geometry of the nullclines to show how small changes in the differences of excitability could lead to block and a variety of reflected waves. Then we introduced a simple model of excitability with pulse coupling based on the normal form near a saddle-node on an infinite cycle. With this simple model, we were able to derive conditions for reflected waves and show that there exists an instable periodic orbit that forms the core of the reflected waves. Our theoretical results are similar in flavor (but different in implementation) from results on diffusive coupling of excitable systems with heterogeneity (Rinzel and Ermentrout 1998). Similarly, Cytrynbaum and Lewis (2009) used very clever numerical methods to find an unstable periodic orbit in a *homogeneous* diffusively coupled excitable medium. These unstable periodic orbits are the organizing centers for reflected waves; heterogeneity allows the trajectory of the wave to get close to the SM of the periodic orbit and thus produce repetitive activity that returns to rest after several cycles.

Xu et al. (2008) suggest that the reason for compression and reflection is due to a change in inhibition as the wave progresses from V1 to V2. They make this argument based on the fact that reflected waves disappear in the presence of bicuculline which reduces inhibition. We found that reduction of inhibition could also remove reflected waves (see Fig. 3). However, the reduction in our simulations was very small. We would argue that since the regime in parameter for reflected waves is fairly small, it does not take much to push the system out of the regime where reflected waves are possible. We have shown that the amount of inhibition does not contribute that much to the excitability of the medium and thus has little effect on the velocity (compression) and therefore on reflection. Instead, we find that manipulations of the threshold and the recurrent excitation lead to the most robust compression and reflection. Xu et al. (2008) did not find reflected waves when they were spontaneously generated. We can offer several hypotheses. During spontaneous activity, the network my be overall more excitable so that the differences in the excitability between the two visual areas is not enough to create reflected waves. Another possibility is that the thalamic involvement in evoked waves somehow alters the thresholds through possibly feedforward inhibition.

Finally, in this article, we only consider wave traveling between two *homogeneous* media, where the transition between them can be represented by a step function (switch of parameters). The abrupt switch was motivated by the idea that the waves move across different brain regions and that these borders are where the reflections occur. In reality, there are heterogeneities even within regions and these could also alter the ability of waves to propagate and influence the degree of reflection and compression. The general analysis of heterogeneities remains an active area of research.

Acknowledgments The authors thank the Marine Biological Laboratory where this study started. J.G. thanks J. Leo van Hemmen and Magteld Zeitler for comments and discussions. J.G. also thanks the Bernstein Center for Computational Neuroscience-Munich and a grant "Reverse physiology of the cortical microcircuit" from the Computational Life Sciences program by the Netherlands Organisation for Scientific Research (NWO) for funding. B.E. thanks J.-Y. Wu for sharing some unpublished data and the National Science Foundation for partial funding of this work.

References

Bressloff PC (2000) Traveling waves and pulses in a one-dimensional network of excitable integrate-and-fire. J Math. Biol. 40:169–198

Bressloff PC (2001) Traveling fronts and waves propagation failure in an inhomogeneous neural network. Phys D 155:83–100

Bressloff PC, Folias S, Prat A, Li X (2003) Oscillatory waves in hinomogeneous media. Phys Rev Lett 91:178101

Coombes S (2005) Waves, bumps and pattern in neural field theories. Biol Cybern 93:91–108

Coombes S, Laing CR (2011) Pulsating fronts in periodically modulated neural field models. Phys Rev E 83:011912

Cytrynbaum E, Lewis T (2009) A global bifurcation and the appearance of a one-dimensional spiral wave in excitable media. SIAM J Appl Dyn Syst 8:348

Ermentrout B, Kleinfeld D (2001) Parabollic bursting in an excitable system coupled with a slow oscillation. Neuron 29:33–44

Ermentrout B, Kopell N (1986) Parabollic bursting in an excitable system coupled with a slow oscillation. SIAM J Appl Math 46: 233–253

Ermentrout B, Rinzel J (1996) Reflected waves in a inhomogeneous excitable medium. SIAM J Appl Math 56:1107–1128

Ermentrout G, McLeod J (1991) Existence and uniqueness of travelling waves for a neural network. Proc R Soc Edimb 434:413–417

Folias S, Bressloff P (2005) Stimulus-locked traveling waves and breathers in an excitatory neural network. SIAM J Appl Math 65:2067–2092

Golomb D, Ermentrout GB (2001) Bistability in pulse propagation in networks of excitatory and inhibitory populations. Phys Rev Lett 86:4179–4182

Golomb D, Ermentrout GB (2002) Slow excitation supports propagation of slow pulses in networks of excitatory and inhibitory populations. Phys Rev E Stat Nonlin Soft Matter Phys 65:061, 911

Hoppensteadt F, Izhikevich E (1997) Weakly connected neural networks, vol 126. Springer Verlag, New York

Hutt A, Atay F (2006) Effect of distributed transmission speeds on propagating activity in neural populations. Phys Rev E 73:021906

Kilpatrick ZP, Folias SE, Bressloff PC (2008) Traveling pulses and wave propagation failure in inhomogenous neural media. SIAM J Appl Dyn Syst 7:161–185

Kilpatrick Z, Bressloff P (2010) Spatially structured oscillations in a two dimensional excitatory neuronal network with synaptic depression. J Comput Neurosci 28:193–209

Osan R, Rubin J, Ermentrout B (2002) Regular traveling waves in a one-dimensional network of theta neurons. SIAM J Appl Math 62(4):1197–1221 (electronic)

Ozeki H, Finn IM, Schaffer ES, Miller KD, Ferster D (2009) Inhibitory stabilization of the cortical network underlies visual surround suppression. Neuron 62(4):578–592

Pinto D, Patrick S, Huang W, Connors B (2005) Initiation, propagation, and termination of epileptiform activity in rodent neocortex in vitro involve distinct mechanisms. J Neurosci 25:8131–8140

Pinto DJ, Ermentrout GB (2001) Spatially structured activity in synaptically coupled neuronal networks. I. Traveling fronts and pulses. SIAM J Appl Math 62(1):206–225 (electronic)

Prat A, Li YX, Bressloff P (2005) Inhomogeneity-induced bifurcation of stationary and oscillatory pulses. Phys D 202(3–4):177–199

Rinzel J, Ermentrout B (1998) Analysis of neural exictability and oscillations. In: Koch C, Segev I (eds) Method in neuronal modeling. MIT press, Cambridge, pp 251–291

Shusterman V, Troy W (2008) From baseline to epileptic activity: A path to synchronized rhythmicity in large-scale neural networks. Phys Rev E 77:061911

Wu J, Huang X, Zhang C (2007) Propagating waves of activity in the neocortex: what they are, what they do. Neuroscientist 55:119–129

Xu W, Huang X, Takagaki K, Wu J (2008) Compression and reflection of visually evoked cortical waves. Neuron 14:487–502